Construction and Building Materials 378 (2023) 131028

Contents lists available at ScienceDirect

Construction and Building Materials

journal homepage: www.elsevier.com/locate/conbuildmat

Investigating the hydration of C_3A in the combined presence of anhydrite and limestone using solid-state NMR, XRD and TG techniques

Valentino Merlo [a,*], Leonardo Marchese [b], Daniela Gastaldi [a], Enrico Boccaleri [c,d,*], Fulvio Canonico [a], Geo Paul [b]

[a] Built - Buzzi Unicem Innovation Lab and Technology, Via Restano 3, 13100 Vercelli, Italy
[b] Dipartimento di Scienze ed Innovazione Tecnologica, Università del Piemonte Orientale A. Avogadro, viale T. Michel 11, 15121 Alessandria, Italy
[c] Dipartimento per lo Sviluppo Sostenibile e la Transizione Ecologica, Università del Piemonte Orientale A. Avogadro, piazza S. Eusebio 5, 13100 Vercelli, Italy
[d] UPO4Sustainability Center, Viale T. Michel 11, 15121 Alessandria, Italy

ARTICLE INFO

Keywords:
AFm
NMR
XRD
Anhydrite
Limestone
C_3A
Hydration
Ettringite

ABSTRACT

Diverse AFm phases are commonly found during the hydration of calcium sulfoaluminate (CSA), Portland (OPC), and calcium aluminate (CAC) cements. Due to the flexibility in their layered double hydroxide (LDH) structure, they are observed in variable single or multi-anion bearing forms, water contents and transient states. When multiple sulfate and carbonate anion sources, in variable compositions, are available during the hydration of cements, the identity, quantity, and stability of the formed AFm phases vary considerably. They may also precipitate as microcrystalline and/or amorphous phases, rendering their detection by X-ray powder diffraction (PXRD) difficult. In this study the AFm phases have been generated through the hydration of tricalcium aluminate (C_3A) in the presence of sulfate (anhydrite) and carbonate ions (limestone) in various compositions. A multi-technique approach involving solid-state nuclear magnetic resonance spectroscopy (ssNMR), thermogravimetric analysis/differential scanning calorimetry (TGA/DSC) and PXRD has been employed to govern the sequence of hydration reactions, the evolution, structure, and the stability of AFm phases at 1 and 28 days of C_3A hydration. The results show that the identity and quantity of AFm phases formed vary considerably according to the nature of the anion sources available during the hydration. Hydration products such as crystalline C_3AH_6, ettringite and amorphous as well as crystalline/microcrystalline monoanionic AFm phases (monosulfate, monocarbonate, hydroxy-AFm) and bi-anionic phases (hemicarbonate and solid-solutions involving more anions) have been identified and quantified.

1. Introduction

Al_2O_3 – Fe_2O_3 – Monosulfate (AFm) phases belong to the layered double hydroxide family whose structure derives from brucite. The general structure of AFm phases are built up of positively charged main layers composed of divalent and trivalent cation hydroxides of the formula $[M^{II}_{1-x}M^{III}_{x}(OH)_2]^{x+}$ and an interlayer gallery accommodating negatively charged anions and water molecules of the formula $[A^{n-}_{x/n}\cdot zH_2O]^{x-}$ where A is either a monovalent anion or half of a divalent anion. During the cement hydration, the divalent and trivalent cations generally present are Ca and Al, respectively. However, other types of cations such as Mg and Fe may also be present. Similarly, anions such as OH^-, Cl^-, CO_3^{2-}, SO_4^{2-} etc. are commonly found in AFm phases in a cement paste [1–5].

Being one of the important constituents of Portland and calcium sulfoaluminate cements, tricalcium aluminate (C_3A) plays a crucial role in the hydration, workability, setting and durability of cement and thus of concrete. The properties of the cement pastes are directly linked to its hydration products and their microstructure development. C_3A hydration results in the formation of various aluminate hydrates and AFm phases [1–5]. The reactions involving the hydration of pure C_3A[1] in the absence of any anion can be summarized as follows.

$$2C_3A + 21H \rightarrow C_4AH_{13} + C_2AH_8 \rightarrow 2C_3AH_6 + 9H \quad (1)$$

* Corresponding authors at: Built - Buzzi Unicem Innovation Lab and Technology, Via Restano 3, 13100 Vercelli, Italy (V. Merlo); Dipartimento per lo Sviluppo Sostenibile e la Transizione Ecologica, Università del Piemonte Orientale A. Avogadro, piazza S. Eusebio 5, 13100 Vercelli, Italy (E. Boccaleri).
E-mail addresses: vmerlo@buzziunicem.it (V. Merlo), enrico.boccaleri@uniupo.it (E. Boccaleri).

[1] Note that the standard cement nomenclature is followed here, whereby C = CaO, S = SiO_2, A = Al_2O_3, $\overline{S}$ = SO_3, $\overline{C}$= CO_2 and H = H_2O.

https://doi.org/10.1016/j.conbuildmat.2023.131028
Received 26 August 2022; Received in revised form 1 February 2023; Accepted 10 March 2023
Available online 28 March 2023

$$2C_3A + 27H \rightarrow C_4AH_{19} + C_2AH_8 \rightarrow 2C_3AH_6 + 15H \quad (2)$$

The highly hydraulic C_3A reacts instantaneously with water resulting in calcium aluminate hydrates (hydroxy-AFm phases) such as C_4AH_{13}, C_4AH_{19} and C_2AH_8, that is responsible for flash setting of cement. When setting in cement paste occurs spontaneously, loss of workability and failure of strength development results consequently. However, these hydroxy-AFm phases are thermodynamically metastable and might convert into a fully hydrated stable phase C_3AH_6 (hydrogarnet) [6–8]. In a real-world cement paste, some hydroxy-AFm phases are still detected.

In order to prevent the flash setting in cement, inter-grinding or addition of proper dosage of calcium sulfate (gypsum and/or anhydrite) to clinker is carried out. The amount of calcium sulfate influences the hydration rate as well as the hydration products of C_3A. The reactions involving the hydration of gypsum and C_3A can be summarized as follows.

$$C_3A + 3C\overline{S}H_2 + 26H \rightarrow C_6A\overline{S}_3H_{32} \quad (3)$$

$$C_6A\overline{S}_3H_{32} + 2C_3A + 4H \rightarrow 3C_4A\overline{S}H_{12} \quad (4)$$

$$C_3A + C\overline{S}H_2 + 10H \rightarrow C_4A\overline{S}H_{12} \quad (5)$$

In the presence of gypsum, highly hydraulic C_3A still reacts extremely fast with water, however, mineral ettringite is formed (equation (3). If insufficient gypsum is present or if exhausted, then the ettringite will react with excess C_3A to form the AFm mineral calcium monosulfoaluminate hydrate (monosulfate) according to equation (4). In addition, the type of calcium sulfate (gypsum, hemihydrate or anhydrite) employed in the binary composition can influence the resulting calcium aluminate hydrates as well as the actual mole ratio between calcium sulfate and C_3A in the cement control the setting characteristics [9,10]. Under certain conditions (i.e. in under-sulfated system), the hydration of C_3A in presence of gypsum can result in the direct precipitation of monosulfate without the formation of ettringite (Equation (5). Moreover, the presence of quicklime in combination with $CaSO_4$ can also influence the C_3A hydration rate and the formation of calcium aluminate hydrates [11]. The other types of sulfates (anhydrite or hemihydrate) will follow similar reaction routine mainly based on the availability of sulfate.

The other most common conditions that alter the nature, evolution and microstructures of C_3A hydration products are the presence of other anions, particularly carbonates (limestone) in cement. Limestone can also be added to the clinker (up to 35%) either to control the setting time or as a SCM [12]. Limestone can either participate in the hydration reactions or act as an inert filler. The reactions involving the hydration of C_3A and $CaCO_3$ binary system can be summarized as follows.

$$C_3A + C\overline{C} + 11H \rightarrow C_4A\overline{C}H_{11} \quad (6)$$

$$2C_3A + C\overline{C} + 12H \rightarrow 2C_4A\overline{C}_{0.5}H_{12} \quad (7)$$

In the presence of excess of $CaCO_3$, the hydration of C_3A leads to the formation of another AFm phase calcium monocarboaluminate hydrate (monocarbonate), probably through the rapid reaction with hydroxy-AFm phases, preventing the generation of hydrogarnet (equation (6) [7,13,14]. However, when insufficient amount of $CaCO_3$ is present during the hydration of C_3A, a transitionally stable AFm phase, hemicarbonate, can appear in this system (equation (7). The availability of dissolved carbonates in the system can destabilize hemicarbonate and a gradual conversion into monocarbonate can be expected [15,16].

A combination of gypsum and $CaCO_3$ in suitable proportions has been effectively used to control the C_3A setting time [17]. Presence of varying amounts of calcium sulfate and calcium carbonate in a ternary formulation alters the phase composition of hydrated C_3A paste due to the formation of sulfoaluminate and carboaluminate AFm phases. Among them, the most expected AFm phases are monosulfate, monocarbonate, hemicarbonate, hemisulfate, and hydroxy-AFm phases. In addition, solid-solutions involving hydroxyls, sulfates and carbonates are predicted. A thorough understanding of the development of AFm phases, their transitional stability as well as their long-term co-existence are important when considering the various applications of C_3A based cements.

Nowadays, the use of anhydrite and limestone in cements become frequent due to either economic, environmental or sustainability reasons. In countries such as China, who accounts for more than 50% worlds' cement production, availability of natural anhydrite for cheaper prices contribute to the replacement of gypsum in Portland cement [9,18]. Similarly, European cement standard regulations (EN 197–1) identifies six types of limestone cements containing, 6–20% (CEM II/A-L, CEM II/A-LL and CEM II/A-M) and 21–35% limestone (CEM II/B-L, CEM II/B-LL and CEM II/B-M), that can be used in structural concrete, highlighting it as an attractive material due to its low processing costs and unlimited availability [19].

Aluminium is a fundamental building block for various types of AFm minerals formed during the hydration of cement. Various AFm phases involving anions such as hydroxyl, sulfate, carbonate, chloride, aluminosilicate etc possess aluminium in their structure [20–25]. Given the importance of aluminate minerals in cement hydration chemistry, NMR spectroscopic study of ^{27}Al nucleus can provide unique insight about reactivity and structure through the determination of its local environments (Table S1) [26]. Monoanionic AFm phases (monosulfate, monocarbonate, hydroxy-AFm) and bi-anionic phases (hemicarbonate and solid-solutions involving more anions) may be precipitated as either microcrystalline or amorphous species in cement pastes, rendering their detection by PXRD difficult. Due to its unparalleled ability to equally detect and quantify amorphous, crystalline, disordered phases and surface species, solid-state NMR spectroscopy is an ideal tool for the investigation of AFm phases.

In this study, various AFm phases are prepared by the hydration of synthetic C_3A in the presence, absence and co-presence of anhydrite and limestone, with a view to investigate the formation and evolution of OH^-, CO_3^{2-} and SO_4^{2-} AFm phases in the hydrated system. An integrated approach involving well-established technique of ^{27}Al solid-state NMR spectroscopy, X-ray powder diffraction and thermogravimetric analysis/differential scanning calorimetry is employed for the characterization of the different crystalline/microcrystalline/amorphous AFm phases. The coupling of complementary techniques supports the combined identification and quantification of crystalline, microcrystalline, and disordered AFm phases in cement pastes in an unprecedented detail.

2. Materials and methods

2.1. Materials

Pure C_3A was prepared in the laboratory according to the procedure reported previously [27]. Calculated amounts of reagent grade (Sigma/Aldrich) calcium carbonate ($CaCO_3$) and aluminium hydroxide ($Al(OH)_3$), were mixed with water to prepare a paste which was then fired into a tubular furnace. The mixture was sintered at 1440 °C for 40 min. The purity of the obtained cubic C_3A was determined by PXRD (Figure S1).

Before the hydration procedure, powdered cubic C_3A along with anhydrite or limestone (supplied by Buzzi Unicem) or both were thoroughly mixed. Pastes were prepared with deionized milliQ water and mixed at 400 rpm in a vertical mixer for 5 min with water to solid ratio (W/B) of 0.4 at 20 °C. Composition of the samples are given in Table 1. C_3A alone was also hydrated for comparison purpose (sample C100_S0_L0). The levels of anions (sulfates and carbonates) were chosen so as to control the amount of AFm phases such as monosulfate or monocarbonate in samples C93_S7_L0, C67_S33_L0 and C73_S0_L27, respectively. C72_S13_L15 was considered as a combined sulfate-carbonate system. The pastes were poured into plastic tubes, sealed immediately after mixing and stored at room temperature. Specimens of

Table 1
Composition (in wt%) of the samples.

Sample Name	C_3A	Anhydrite	Limestone
C100_S0_L0	100	0	0
C93_S7_L0	93	7	0
C67_S33_L0	67	33	0
C73_S0_L27	73	0	27
C72_S13_L15	72	13	15

hydrating pastes were picked after 1 and 28 days. Sampling was performed by breaking a fragment of the paste which was immediately transferred into a desiccator under nitrogen at 40 °C for 24 h. The treatment was required to stop the hydration by removing free water and to reduce interaction with external agents such as CO_2. Dried pastes were then manually ground in agate mortar and analysed.

2.2. Solid-state NMR

Solid-state NMR spectra were acquired with a wide bore 11.75 Tesla magnet on a Bruker Avance III 500 spectrometer using operational frequencies for ^{1}H and ^{27}Al of 500.13 and 130.32 MHz, respectively. A 4 mm triple resonance probe, in double resonance mode, with magic angle spinning (MAS) was employed in all the experiments and the samples were packed on a Zirconia rotor and spun at a MAS rate of 15 kHz. The ^{27}Al 1D MAS spectra have been acquired on large sweep width with small pulse angle ($\pi/12$) to ensure quantitative interpretation [28]. In addition, central transition ^{27}Al MAS NMR spectra were acquired under high power ^{1}H decoupling conditions. The delay, d1, between accumulations was 1 s and the chemical shifts are reported using δ scale and are externally referenced to $Al(H_2O)_6^{3+}$ ion in 1.0 M $AlCl_3$ solution to 0.0 ppm.

All NMR spectra were fitted (DMFIT) for quantitative deconvolution of overlapping peaks [29]. The lineshape of the peaks associated with calcium aluminate hydrates was described by a Gaussian and/or Lorentzian function except for monocarbonate and AFm*, where quadrupolar lineshapes were employed [30,31]. Quadrupolar coupling parameters and chemical shift values of most common aluminate phases in hydrating cement systems have already been reported in the literature and were used for the quantitative deconvolution study (Refer to Table S2).

2.3. Powder XRD

PXRD analyses were performed on a Bruker AXS D4 Endeavor diffractometer working in Bragg-Brentano geometry, equipped with a ceramic X-ray tube KFF (Cu Kα radiation) and a “Linx Eye” dispersive detector. The acquisition of diffraction patterns was performed in the 8-55° 2θ range at 0.02° 2θ step size and 0.5 sec time/step; during the acquisition the sample was continuously spun at 30 rpm [21]. Samples of pastes were ground and pressed in pellet through a Polysius Automatic Sample Preparation Module (APM).

Semi-quantitative mineralogical analyses were conducted by Rietveld method using the Topas 2.0 package (software were commercially supplied by Bruker AXS). The refinements were conducted in the whole 8-55° 2θ range by using a 5th order Chebychev Polynomium for the background calculation and allowing refinement of the sample displacement; crystal size of all structures was set free to vary between 32 and 500 nm while preferred orientations were avoided thanks to automatic sample preparation; Rwp (Residual weighted profile) value was in all cases lower than 10% and estimated average error of refinement was lower than 2%.

2.4. Tg/dsc

Thermogravimetric/Differential Scanning Calorimetric (TG/DSC) measurements were performed on paste fragments by means of a Mettler Toledo TG/DSC 1: thermal ramp was set from 35 to 950 °C at 20 °C/min in 80 mL/min air flow; 90 μL alumina pans were used.

3. Results

3.1. Hydration of C_3A alone

Fig. 1A shows the ^{27}Al central transition MAS NMR spectra of anhydrous cubic C_3A sample along with the deconvoluted spectrum with individual contribution from each ^{27}Al site. There are two crystallographically distinct tetrahedrally coordinated ^{27}Al sites present in the cubic C_3A with similar isotropic chemical shift values as well as quadrupolar coupling parameters and is in agreement with earlier reports [5,8]. Note that the peak area belonging to these two tetrahedral Al sites cover the entire chemical shift range associated with the tetra- (80–45 ppm), penta- (40–25 ppm) and octa- (15 – 0 ppm) coordinated aluminium sites, rendering the spectral assignments of hydrated aluminates complicated [32]. During the hydration of C_3A, in the absence of any anions, various AFm calcium aluminate hydrates are formed (Equation (1) and (2). The stability of the hydrates is usually influenced by the relative humidity and temperature as hydroxy-AFm phases are initially formed which would get converted into a more stable hydrogarnet. The ^{27}Al central transition MAS NMR spectra recorded with proton decoupling from the paste hydrated for 1 and 28 days are shown in Fig. 1B, together with the corresponding fitted spectra and their individual components from each ^{27}Al site. According to the position of the chemical shifts, it is possible to state that the main hydration product is hydrogarnet (C_3AH_6, 12.3 ppm) in both the cases. However, traces of hydroxy-AFm phases (10.4 ppm) (C_4AH_{13}, C_4AH_{19} and C_2AH_8) are present. Relative proportion of the population distribution of ^{27}Al sites in the hydrated C_3A are given in Table 2. According to Sanchez-Herrero et al., immediate stabilization of the paste with the formation of C_3AH_6 can be achieved by the use of a low liquid/solid ratios [33].

It is important to note here that the resonance peaks associated with hydrogarnet and hydroxy-AFm phases exhibited narrower resonances (without the quadrupolar broadening) making the deconvolution and quantification rather straightforward. Within the first 24 h, around 80% of C_3A has been subjected to hydration which would increase up to 97% after 28 days. Although around 8% of aluminium nuclei belongs to hydroxy-AFm phases at early hydration stages, their level diminished greatly with increasing hydration time, and they have been eventually converted to stable hydrogarnet at 28 days which is the dominant phase.

The formation of AFm phases during C_3A hydration could also be followed by powder X-ray diffraction (Fig. 2A). The identity and distribution of phases in hydrated C_3A has been verified by Rietveld refinement and is shown in Table 3. The main hydration product is C_3AH_6 (main peak at $2\theta = 17.2°$, corresponding to reflection 211), in addition traces of hydroxy-AFm phases are detected (peaks at 10.9° and 11.4° 2θ). The presence of two peaks generally ascribed to hydroxy-AFm is due to the variable nature of this phase, that can be described either as C_4AH_{13} or C_4AH_{19} or C_2AH_8. As the hydration progressed up to 28 days, only less than 2% of residual anhydrous cubic C_3A remained in the sample where 97% accounted for C_3AH_6. Moreover, the thermal behavior of the AFm phases has been studied (Fig. 2B): sample C100_S0_L0 shows major endothermic signals in two consecutive steps associated with the weight loss due to dehydration at around 340 °C and 485 °C and is in agreement with the patterns reported in the literature for C_3AH_6 [34]. In addition, a small weight loss at around 180 °C is visible and is due to dehydration of hydroxy-AFm phases.

3.2. Hydration of C_3A in presence of calcium sulfate

Blends of cubic tricalcium aluminate with two different amounts of anhydrite has been hydrated for 1 and 28 days and evaluated via ^{27}Al MAS NMR spectroscopy (Table 1). Fig. 3 shows the ^{27}Al central

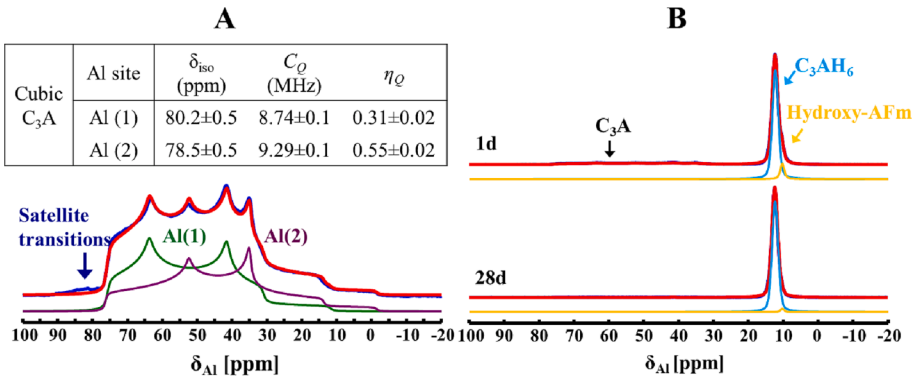

Fig. 1.. ^{27}Al central transition MAS NMR spectrum (blue) for anhydrous (A) and hydrated (B) cubic C_3A obtained with ^{1}H decoupling along with the deconvoluted spectra (red) and individual contribution from each ^{27}Al site. δ_{iso} = isotropic chemical shift, C_Q = quadrupolar coupling constant and η_Q = asymmetry parameter of the electric field gradients. (For interpretation of the references to colour in this figure legend, the reader is referred to the web version of this article.)

Table 2
Relative proportion of the population distribution of AFm phases through ^{27}Al sites from the MAS NMR data in different hydrated C_3A blends (estimated error ± 2%). E1 and E2 = ettringite, Ms = monosulfate, Mc = monocarbonate, Hy-AFm = hydroxy-AFm phases, AFm* = other AFm phases, SEF = secondary ettringite formed.

		^{27}Al Species (wt%) Al^{IV} C_3A	Al^{VI} C_3AH_6	E1	E2	Ms	Hy-AFm	AFm*	Mc	SEF
C100_S0_L0	**1d**	20	72	–	–		8	–	–	–
	28d	3	96	–	–		1	–	–	–
C93_S7_L0	**1d**	31	42	–	–	9	18	–	–	–
	28d	28	48	–	–	16	8	–	–	–
C67_S33_L0	**1d**	36	31	4.5	4.5	8	16	–	–	–
	28d	36	23	7.5	7.5	14	12	–	–	–
C73_S0_L27	**1d**	22	25	–	–	–	–	20	33	–
	28d	13	24	–	–	–	–	20	43	–
C72_S13_L15	**1d**	38	13	2.5	2.5	5	–	25	8	6
	28d	28	15	1.5	1.5	6	–	28	10	10

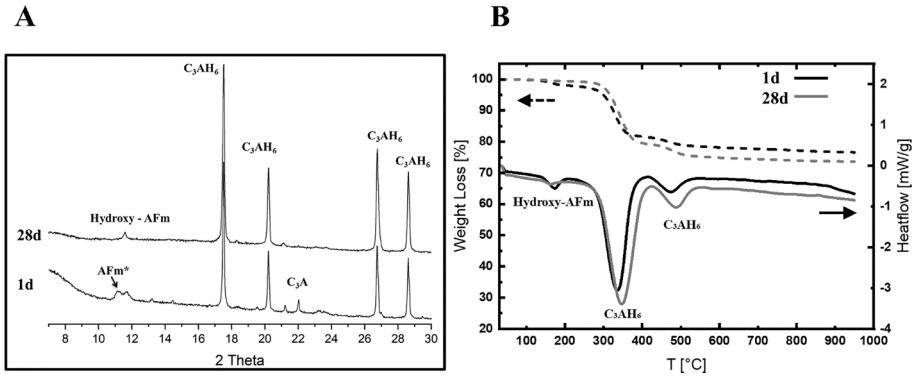

Fig. 2. Powder X-ray diffraction patterns (A) and TG/DSC evaluation (B) of sample C100_S0_L0 hydrated at 20 °C with W/B = 0.4.

transition MAS NMR spectra recorded with proton decoupling of various anhydrite based hydrated C_3A pastes. When low amount of anhydrite has been used (sample C93_S7_L0), the C_3A hydration products were AFm phases, calcium monosulfoaluminate (monosulfate) and the hydroxy-AFm along with C_3AH_6. Here, monosulfate appeared as narrow peak with δ_{cg} at 9.7 ppm (see supplementary data). After 1 day, C_3AH_6 and hydroxy-AFm have been the dominant hydrated phases (Table 2). The formation of monosulfate has been retarded at this stage and could be related to a faster formation of hydroxy-AFm phases. ^{27}Al NMR revealed that no changes in the type of hydrated phases occurs within 28 days, although the relative intensities of the peaks and therefore the quantity of these phases did vary: after 28 days, more monosulfate is formed at expenses of hydroxy-AFm phases.

It is important to note here that even at this stage of hydration, major amounts of anhydrous C_3A remain (28%), probably related to either the low W/B ratio used or due to the coating of precipitates of hydrated aluminates and/or calcium and sulfate ions on the C_3A grains which prevented its hydration further. Indeed, there are few studies that provided various insights on the retardation of C_3A hydration in the presence of calcium sulfate [35,36]. Moreover, ettringite has been never detected at any stages of hydration in this composition presumably due to the lack of sulfate in the system. C_3AH_6 being crystallized in a cubic phase, the ^{27}Al nucleus residing in an extremely symmetrical environment would experience a relatively negligible quadrupolar interactions and expected to show a narrow resonance peak. However, the relatively broader peak detected for C_3AH_6 could be attributed to the chemical shift distribution originating from its growth as a shell around the wider C_3A grain boundaries [37].

Table 3
Mineralogical composition in weight (%) of the different AFm phases formed during the hydration of C_3A blends at different aging times obtained by means of semi-quantitative Rietveld refinement on PXRD patterns (estimated error ± 2%). HT = hydration time, E = ettringite, Ms = monosulfate, Mc = monocarbonate, Hc = hemicarbonate, Hy-AFm = hydroxy-AFm phases, AFm* = other AFm phases, MH = monohydrocalcite, An = anhydrite, L = calcite, OP = other phases.

	Phases (wt%)											
	HT	C_3A	C_3AH_6	E	Hy - AFm	AFm*	Ms	MH	Hc	Mc	An	L	OP
C100_S0_L0	1d	14.4	77.1	–	2.8	5.7	–	–	–	–	–	–	–
	28d	1.3	97.3	–	1.4	–	–	–	–	–	–	–	–
C93_S7_L0	1d	20.6	53.4	–	14.8	–	5.5	–	–	–	1.5	4.2	–
	28d	18.0	52.0	–	9.9	1.0	13.7	–	–	–	–	2.3	2.9
C67_S33_L0	1d	19.3	18.8	23.0	20.5	–	1.7	–	–	–	13.0	3.8	–
	28d	19.3	14.7	30.5	9.6	–	14.0	–	–	–	7.5	4.4	–
C73_S0_L27	1d	9.5	19.5	–	–	–	–	3.1	7.6	15.4	–	37.8	7.2
	28d	6.8	26.8	–	–	–	–	3.8	8.6	18.2	–	29.4	6.5
C72_S13_L15	1d	19.0	20.5	9.0	10.0	–	2.5	3.0	7.2	3.5	1.8	19.9	3.4
	28d	14.3	18.9	11.9	9.1	–	9.8	1.8	7.9	6.5	1.5	12.8	5.5

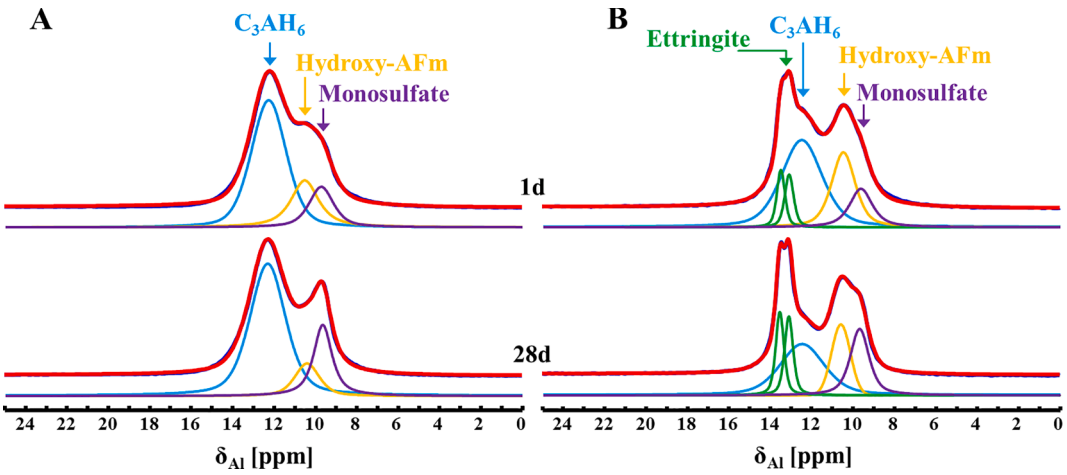

Fig. 3. ^{27}Al central transition MAS NMR spectra (octahedral region) for the hydrated C93_S7_L0 (A) and C67_S33_L0 (B) obtained with ^{1}H decoupling along with the deconvoluted spectra and individual contribution from each ^{27}Al site.

For the composition with higher amounts of anhydrite (sample C67_S33_L0), the hydration of C_3A leads to major differences in the quantity and distribution of aluminate hydrates as noted in Fig. 3B. Ettringite has been detected here from the beginning of hydration and the amount formed has increased as the hydration progressed. There have been two distinct ^{27}Al resonances detected for ettringite in this sample at 13.1 and 13.5 ppm highlighting the highly symmetrical aluminium sites in a well crystallised sample [38,39]. Besides ettringite, presence of AFm phases monosulfate and hydroxy-AFm along with C_3AH_6, have also been noted. A decrease in the amount of hydrogarnet has been noted here as we go from 1 to 28 days (Table 2), presumably due to reactions (8) and (9).

$$C_3AH_6 + 3C\bar{S} + 26H \rightarrow C_6A\bar{S}_3H_{32} \quad (8)$$

$$C_3AH_6 + C\bar{S} + 6H \rightarrow C_4A\bar{S}H_{12} \quad (9)$$

A significant C_3A dissolution inhibition (36 %, Table 2) has been noted, much higher than in sample C93_S7_L0: in fact, the level of residual anhydrous C_3A showed no change between 1 and 28 days of hydration. Presence of additional anhydrite being the only difference from sample C93_S7_L0, pronounced C_3A hydration inhibition could be due to the existence of further calcium and sulfate ions on the C_3A grains

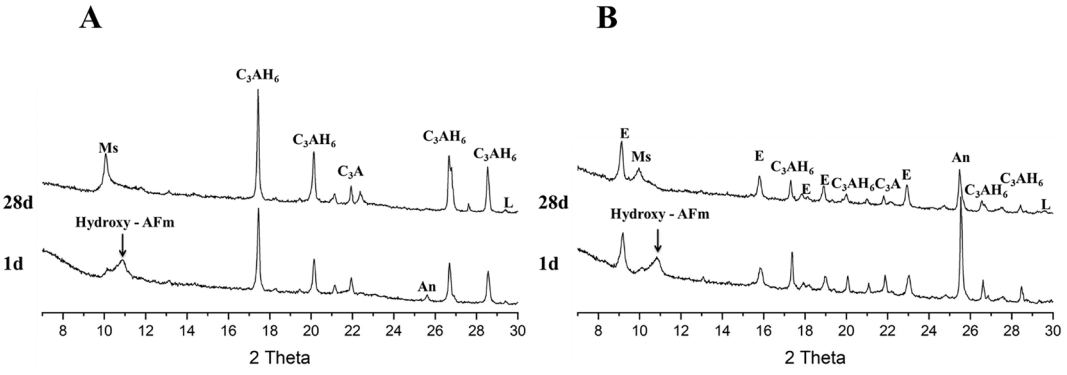

Fig. 4. Powder X-ray diffraction patterns of samples C93_S7_L0 (A) and C67_S33_L0 (B) hydrated at 20 ℃ with W/B = 0.4. Ms = Monosulfate, E = ettringite, C$ = anhydrite.

preventing its access to water. On the other hand, majority of the water is stored in highly hydrated phases such as ettringite and monosulfate leading to water deficiency.

Fig. 4 presents the evolution of the PXRD patterns of the samples C93_S7_L0 and C67_S33_L0 after 1 and 28 days of hydration, confirming that the hydration of C_3A in the presence of anhydrite leads to a very rapid formation of hydrated calcium sulfoaluminate phases. Depending on the amount of anhydrite, different calcium sulfoaluminate hydrates have been produced during the hydration: when a very low amount of anhydrite has been used, as in sample C93_S7_L0, the diffraction patterns have been dominated by monosulfate (peaks at 9.9° 2θ, reflection 003) and hydroxy-AFm as well as C_3AH_6. Although the peaks attributed to anhydrous C_3A diminished in intensity over time due to hydration, significant amount of residual anhydrous C_3A has still been detected even after 28 days in this sample (Table 3). The development of monosulfate is probably due to the favourable conversion from hydroxy-AFm phases, rather than from the further hydration of C_3A.

When a higher amount of anhydrite has been used, as in sample C67_S33_L0, characteristic changes are seen in the PXRD pattern (Fig. 4B) compared to the preceding sample. After 1 day of hydration, the PXRD pattern has been dominated by peaks due to ettringite (peaks at 9.2° 2θ, reflection 100) whose appearance at an early stage confirms its rapid formation in a favourable sulfate ion concentration in the blend; its quantity gradually increases as the hydration progressed to 28 days. Besides ettringite, C_3AH_6, monosulfate and hydroxy-AFm are also identified in this composition. The amounts of C_3AH_6 and hydroxy-AFm diminished greatly with increasing hydration time confirming their gradual conversion to ettringite and monosulfate (Table 3). C_3A hydration is inhibited after 1 day; moreover, anhydrite has been detected throughout the hydration period, albeit in small quantities.

The TGA/DSC patterns of the two samples C93_S7_L0 and C67_S33_L0, after 1 and 28 days of hydration, are shown in Fig. 5. In sample C93_S7_L0 only three major endotherms at around 210, 340 and 480 °C have been noted that are associated with weight losses due to water from hydroxy-AFm and C_3AH_6 (Fig. 5A). The presence of an endotherm close to 220 °C is also visible which is attributed to the loss of water from monosulfate. In sample C67_S33_L0 (Fig. 5B), the sharp endothermal signal at about 155 °C is attributed to the characteristic dehydration of ettringite [40], in addition to the one at around 220 °C, associated with weight loss of water molecules from monosulfate. Moreover, two intense endothermal signals at around 340 °C and 485 °C, attributed to the dehydration of C_3AH_6, have been also confirmed in this sample. Decomposition of hydroxy-AFm phases occurs around 210 °C and their presence cannot be ruled out, being overwhelmed by the strong and large signal of ettringite.

3.3. Hydration of C_3A in combination with limestone and anhydrite

Before discussing the effects of the combined presence of sulfates and carbonates on the AFm phase formations, binary formulation containing only C_3A and limestone is presented (sample C73_S0_L27). The central transition ^{27}Al MAS NMR spectrum recorded with proton decoupling of hydrated sample C73_S0_L27 showed three distinct peaks (Fig. 6A). The assignment of resonance due to C_3AH_6 is straight forward as it appeared as a Gaussian/Lorentzian peak at 12.4 ppm. The assignment of the remaining two peaks has been complicated as they displayed quadrupolar line shapes. Many considerations suggest that the up-field peak (δ_{CG} at 8.6 ppm), which showed characteristic second-order quadrupolar broadening, has been due to calcium carboaluminate AFm phase, monocarbonate [41,42]. The other peak displayed asymmetric lineshape characteristic of the combination of second-order quadrupolar broadening and significant distributions of isotropic chemical shift with δ_{CG} at around 10.6 ppm. Although the broadening observed here could also suggest the presence of some disorder in the phase, this peak is tentatively assigned as AFm* and might be due to the concomitant presence either multiple AFm phases or solid-solutions involving carbonates and hydroxyls. The assignment of this resonance peak will be further clarified while discussing the PXRD data. After 28 days of hydration, the dominant octahedral aluminate phase has been monocarbonate which can be formed directly from C_3A (equation (6) or from C_3AH_6 according to reaction (10).

$$C_3AH_6 + C\overline{C} + 5H \rightarrow C_4A\overline{C}H_{11} \quad (10)$$

The fast formation of AFm phase monocarbonate from C_3A and $CaCO_3$ can be seen from the accompanying Table 2: this phase is the dominant one after 24 h of hydration. While the amounts of AFm* formed in the course of the early stages of hydration remains unchanged, an increase in the monocarbonate phase has been noted. This particular observation is contrary to what has been determined for the three previous compositions where a reduction in hydroxy-AFm phases has been recorded (Table 2). Past reports on the study of C_3A hydration found out that in the presence of $CaCO_3$, the formation of AFm phases C_4AH_{13} and C_2AH_8 is prohibited [43]. Moreover, the amount of anhydrous C_3A detected after 28 days of hydration is much lower (13 %) than that observed for anhydrite based binary compositions (samples C93_S7_L0 and C67_S33_L0). The modulation of C_3A hydration inhibition is probably associated with the presence of carbonate anions which, unlike sulfate anions, are less favourably chemisorbed onto the C_3A grains.

When the rate of hydration in C93_S7_L0/C67_S33_L0 and C73_S0_L27 are compared, an obvious deviation between them is evident and the differences in the anion source is highlighted. The apparent disparity of hydration process is first emerged at early hydration stage where a suppression of C_3A hydration is pronounced in samples C93_S7_L0/C67_S33_L0. On the other hand, C_3A hydration is boosted by the presence of carbonate species as implied by the low content of residual C_3A at 28 days in sample C73_S0_L27. Thus, the adequacy of carbonate ions in the formulation is a crucial step to prevent the inhibition of C_3A hydration. Examination of the hydrated aluminate phases at early hydration stage showcases that the formation of C_3AH_6 is disadvantaged in sample C73_S0_L27 and the trend is continued at 28

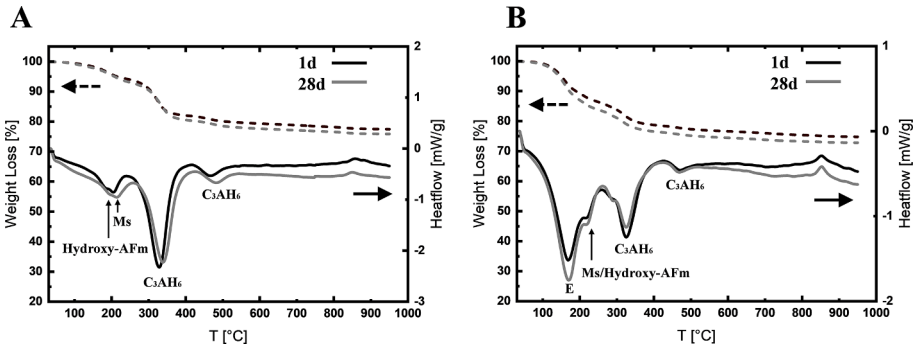

Fig. 5. TG/DSC patterns of sample C93_S7_L0 (A) and C67_S33_L0 (B) hydrated at 20 °C with W/B = 0.4. Ms = Monosulfate, E = ettringite.

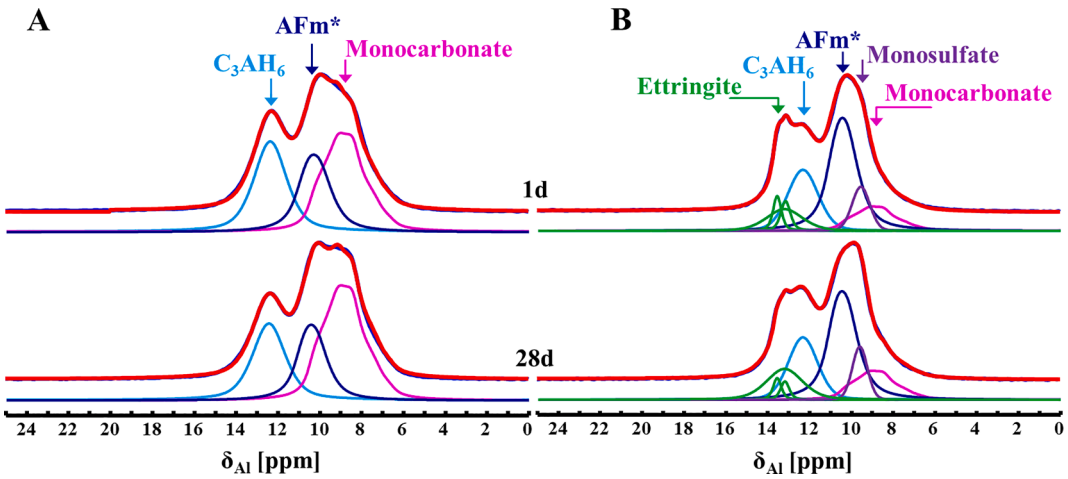

Fig. 6. ^{27}Al central transition MAS NMR spectra (octahedral region) for the hydrated C73_S0_L27 (A) and C72_S13_L15 (B) obtained with ^{1}H decoupling along with the deconvoluted spectra and individual contribution from each ^{27}Al site. AFm* = various AFm phases and/or solid-solutions.

days as well. This can be attributed to the presence of carbonate ions and its concomitant consumption by various calcium aluminate hydrates to precipitate carboaluminate AFm phases.

Proceeding to the system with the concurrent presence of anhydrite and limestone, the formation of AFm phases from the hydration of C_3A is substantially more complicated. The central transition ^{27}Al MAS NMR spectra, recorded with proton decoupling, of sample C72_S13_L15 is shown in Fig. 6B. Characteristic changes have been seen in the ^{27}Al MAS NMR spectra and the products' identities are confirmed with the help of PXRD. Within a narrow chemical shift range of 5 ppm (between 8.5 and 13.5 ppm) at least five different hydrated aluminates (namely ettringite, C_3AH_6 and AFm phases monosulfate, AFm*, and monocarbonate) have been observed in this sample during the whole hydration period under study. According to Glasser and co-workers, several AFm phases, containing OH^-, SO_4^{2-} and CO_3^{2-}, are incompletely miscible with each other and may coexist at 25 °C [44]. AFm* and C_3AH_6 are the main hydrated phases after 1 day, followed by monosulfate and monocarbonate in similar quantities. Small amount of crystalline ettringite has been formed after 1 day as can be seen from the two narrow resonances in the spectra at 13.1 and 13.5 ppm. Moreover, significant amount of monosulfate has been detected at the beginning of hydration with an increase in its content at 28 days. Interestingly, an additional broader peak centred at 13.3 ppm also appears at 1d whose intensity increases at 28 days. Many considerations suggest the broad peak is also associated with ettringite and called secondary ettringite formation (SEF), however, morphologically different from the highly crystalline ettringite mentioned earlier. Its formation can be associated to the delayed dissolution of limestone, which destabilizes various AFm phases and can lead to the formation of secondary ettringite.

Kuzel and Pöllmann have reported similar observations and ascribed them to the instabilities of ettringite during the carbonate hydrate precipitations [45]. Another study using thermodynamic models reported that the stabilization of ettringite can be achieved at the expense of monosulfate by the presence of limestone in Portland-limestone cements through the formation of monocarbonate [46]. The phase distribution is not significantly affected after 28 days: a general increase in all the hydrated phases is observed at the expense of C_3A, whose residual amount is still significantly high.

The PXRD patterns of binary formulation containing only C_3A and limestone, sample C73_S0_L27, is presented in Fig. 7A. The observed pattern is dominated by a single AFm phase with reflections close to that of monocarbonate (peak at 11.8° *2Θ*, reflection 100) and the presence of C_3AH_6 is also confirmed. Formation of carbonate bearing AFm phase monocarbonate is expected in this paste according to equation (6) and it is known that generally metastable hemicarbonate (equation (7) is formed first and gradually converts to monocarbonate with time if excess limestone is present [47].

Contrary to the observation from ^{27}Al NMR data for sample C73_S0_L27, where an additional hydrated aluminate phase (AFm*) has been detected, no other AFm phases, including hemicarbonate or hydroxy-AFm phases, have been detected in the PXRD pattern of hydrated sample C73_S0_L27 at any time of hydration. According to the single crystal structural solution, the structure of AFm phase hemicarbonate is composed of positively charged main layers,

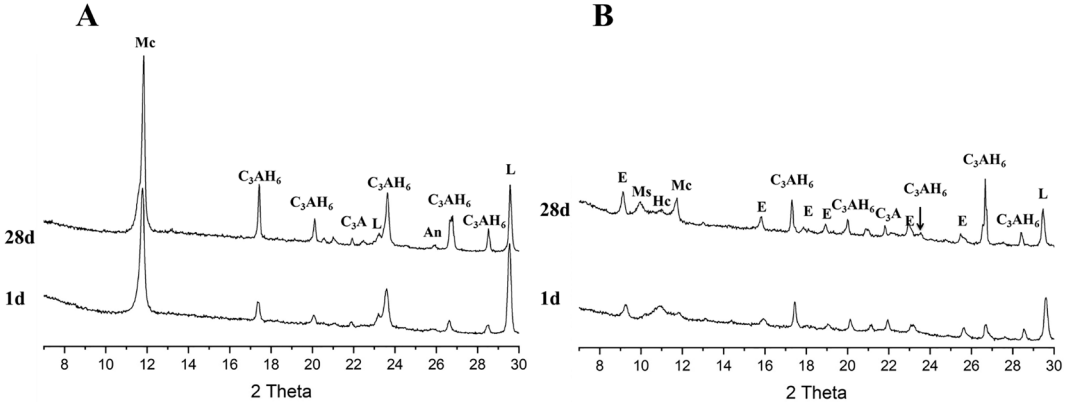

Fig. 7. PXRD patterns of samples C73_S0_L27 (A) and C72_S13_L15 (B) hydrated at 20 °C with W/B = 0.4. Mc = Monocarbonate, E = ettringite, Ms = monosulfate, Hc = hemicarbonate, C = calcite, D = dolomite.

$[Ca_4Al_2(OH)_{12}]^{2+}$, and negatively charged inter-layers where water molecules and statistically distributed carbonate anions are located [48]. The structure of the main layers is typical of the AFm family, therefore, a Lorentzian peak is expected in the ^{27}Al NMR spectrum, similar to hydroxy-AFm or monosulfate. Many of the cementitious phases are poorly crystallized and disordered, therefore, PXRD cannot render satisfactory structural information [20]. Accordingly, it can be stated that AFm* is not a well-crystalline AFm phase.

Based on the classical work by Francois et al. and Renaudin et al., single crystal diffraction studies have revealed two modifications for monocarbonate, ordered- and disordered-$C_4A\hat{C}H_{11}$ structure with different stacking sequences of the layers [49,50]. The arrangement of stacking slab varies: the ordered structure can be regarded as being built from a unique neutral layer $[Ca_4Al_2(OH)_{12}{\cdot}CO_3{\cdot}5H_2O]$, whereas the disordered structure is built from two kinds of layers, one positively charged $[Ca_4Al_2(OH)_{12}{\cdot}4H_2O]^{2+}$ and the other one negatively charged $[Ca_4Al_2(OH)_{12}{\cdot}2CO_3{\cdot}6H_2O]^{2-}$ with different arrangements of water molecules and carbonate groups forming the interlayer region. Moreover, the distances between two adjacent main layers are closely similar in both structures. Such diverse structural arrangements in a disordered phase can give rise to multiple ^{27}Al resonance lines while a very close interlayer distances reveal no differences between two modifications by PXRD [42].

The formation of solid-solutions between hydroxyls and carbonates in the interlayer structure of Al-containing AFm phases are common and can play an important role in stabilizing these solids [44,51]. Besides that, carbonation of AFm phases is a possibility and phases such as carbonated hemicarbonate is also reported [48,52,53]. Therefore, AFm* can be any of the above phases in amorphous form or a combination of phases or solid-solution involving hydroxyls and carbonates, the identity as well as the nature of its formation warrant further studies.

Fig. 7B shows the PXRD pattern of ternary formulation, containing C_3A, anhydrite and limestone, hydrated for 1 and 28 days. The phase analysis shows that the main hydration products are ettringite, C_3AH_6, monosulfate and monocarbonate. Traces of hemicarbonate (peak at 10.8° 2θ) are also visible in this sample, however, its intensity decreased as hydration progressed. Moreover, a continuous solid-solution between hydroxyls, carbonates and/or sulfates cannot be precluded. Significant amount of anhydrous C_3A as well as calcite/dolomite has still been detected even after 28 days of hydration (Table 3). Formation of calcium sulfoaluminate and calcium carboaluminate phases are expected in this ternary system according to equation (11), however, what is important is their mutual presence in the final phase assemblage. It is essential to note that despite the presence of significant amounts of anhydrite and calcite/dolomite in the phase assemblage at 28 days, inhibition of C_3A hydration is still stronger in this ternary formulation.

$$5C_3A + 4C\overline{S} + 2C\overline{C} + CH + 78H \rightarrow C_6A\overline{S}_3H_{32} + C_4A\overline{S}H_{12} + C_4A\overline{C}H_{11} + 2C_4A\overline{C}_{0.5}H_{12} \quad (11)$$

The TGA/DSC patterns of the two samples, C73_S0_L27 and C72_S13_L15, after 1 and 28 days of hydration, are shown in Fig. 8. C73_S0_L27 has a sharp endothermal signal at around 205 °C with two shoulders at 150 °C and 260 °C that corresponds to the loss of water from AFm phases such as AFm* and/or monocarbonate, confirming the formation of considerable amounts of calcium carboaluminate phases, as observed in the PXRD analysis [33]. In addition, two endothermic contributions at around 330 °C and 480 °C due to the dehydration from C_3AH_6 are also visible. C72_S13_L15 shows a continuous loss of water, where few strongly overlapped signals are observed, which are difficult to distinguish. Comparing with the data of previous samples it is possible to assume that the endotherm at 140 °C corresponds to ettringite, while the endotherm at 205 °C corresponds to AFm* or monocarbonate. However, endotherms due to monosulfate are covered in the very same region, therefore, its contribution cannot be completely discounted. The endotherm at 330 °C and 480 °C correspond to C_3AH_6.

3.4. ^{27}Al MAS NMR sideband analysis for AFm phase identification

^{27}Al MAS NMR spectra of the central and satellite transitions at 11.75 T for the various hydrated (28 days) C_3A samples are shown in Fig. 9A. The spectra displayed multiple resonances from the central and satellite transitions (Fig. 9B) with the spinning sideband (ssb) manifold extending over a spectral width ranging from 0.5 to 1.0 MHz. Several overlapping ^{27}Al resonances, displaying very similar chemical shifts and quadrupolar parameters, originating from various AFm phases, makes the spectral assignment challenging. However, some useful information can be derived from the spectral analysis.

The ^{27}Al MAS NMR spectrum of sample C100_S0_L0 showed a single resonance (C_3AH_6) from the central transition (CT, fwhm = 280 Hz) and a complete manifold of ssb extended over a spectral width of 500 kHz (Fig. 9A). It is important to note that no proton decoupling has been applied while recording the spectrum, therefore, contribution from hydroxy-AFm phases cannot be distinguished. Similarly, sample C93_S7_L0 showed two resonances from the central transition and a complete manifold of ssb extended over a spectral width of 660 kHz. The contributions from C_3AH_6 and AFm phases could be distinguished from the center-band of the CT as shown in Fig. 9B, however, separation of the individual AFm phases (hydroxy-AFm and monosulfate) is not possible. For what concerns the sample C73_S0_L27, three resonances from the central transition and two resonances from the − 1st-order spinning sideband from the satellite transition have been clearly visible with manifold of ssb extended over a spectral width of more than 1 MHz. Similar to previous sample, contributions from C_3AH_6 and an AFm phase (monocarbonate) have been clearly distinguishable.

Ettringite has been detected in sample C67_S33_L0 and C72_S13_L15 and appeared as a single resonance in both central transition and from the − 1st-order spinning sideband of the satellite transition which has not been detected beyond 3rd-order ssb demonstrating the presence of a small ^{27}Al quadrupolar coupling. It is essential to note that the ^{27}Al MAS

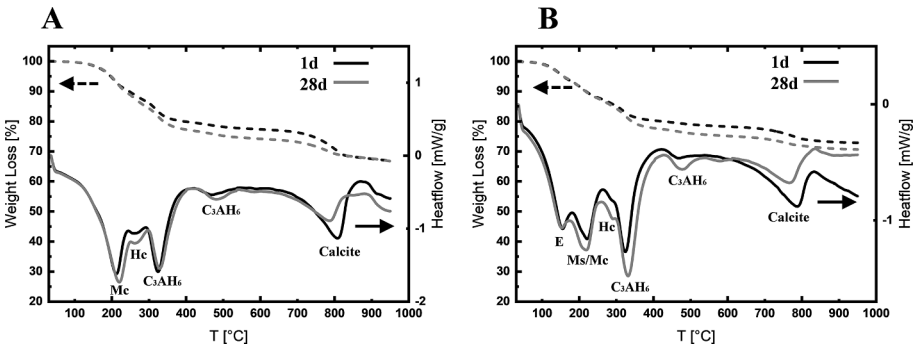

Fig. 8. The thermal analysis with TG/DSC patterns of sample C73_S0_L27 (A) and C72_S13_L15 (B) hydrated at 20 °C with W/B = 0.4. E = ettringite, Mc = monocarbonate, Hc = hemicarbonate, Ms = monosulfate.

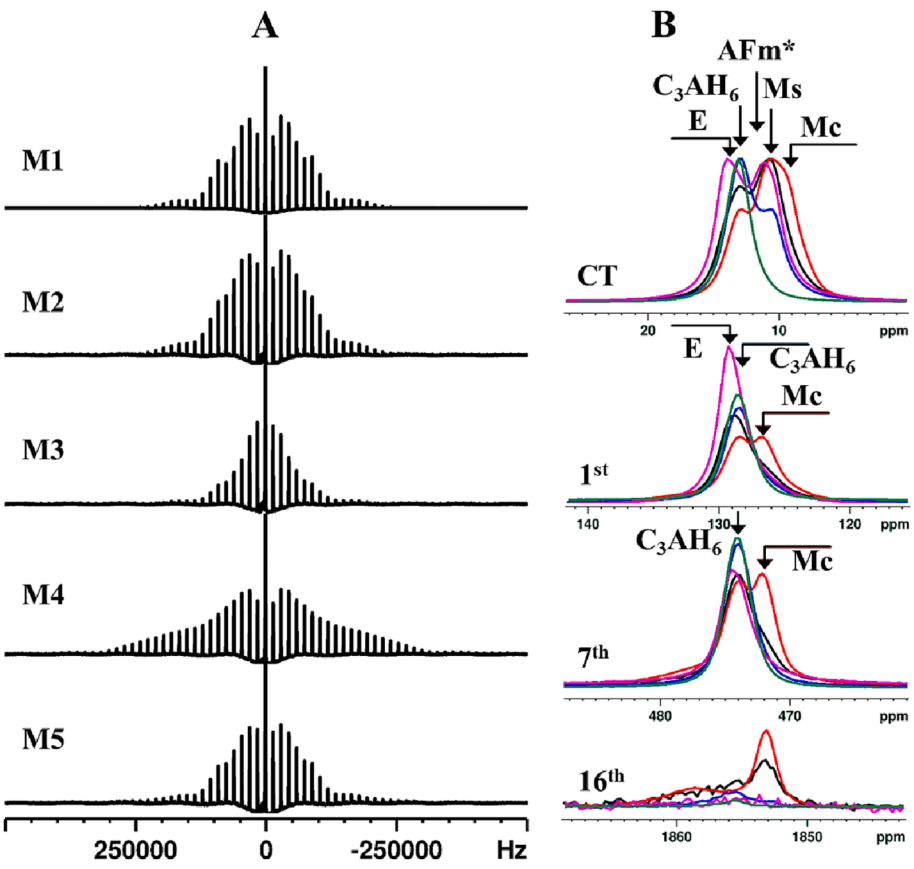

Fig. 9. ^{27}Al MAS NMR spectra of the central and satellite transitions for various hydrated (28 days) C_3A blends obtained without proton decoupling (A) with the expansions of the octahedral region (B) for the central transition (CT) and the line shape for the various-order spinning sideband from the satellite transitions. C100_S0_L0 = green, C93_S7_L0 = blue, C67_S33_L0 = maroon, C73_S0_L27 = red and C72_S13_L15 = black. E = ettringite, Ms = monosulfate, Mc = monocarbonate, AFm* = various AFm phases and/or solid-solutions. (For interpretation of the references to colour in this figure legend, the reader is referred to the web version of this article.)

NMR sideband analysis does not allow the distinction of overlapping resonances from certain AFm phases in complex phase compositions. These AFm phases include hemicarbonate, hydroxy-AFm phases and the entire range of solid-solutions involving any composition of hydroxyls, sulfates and carbonates (Table S2).

4. Discussion

C_3A hydration alone leads to the fast formation of metastable AFm phases hydroxy-AFm that would get converted to stable hydrogarnet which induces stiffening of the hydrated paste. Hydration of C_3A becomes complete with time when the right amount of water is employed. However, with the addition of calcium sulfate, inhibition of C_3A hydration is ensued. Recently, some detailed considerations have been given to the understanding of the factors which control the kinetics of the hydration of C_3A in presence of $CaSO_4$ [35,36]. Many of the key questions concerning these areas include the impact of the type of sulfate source used and its significance in the kinetics of the hydration of C_3A. It became clear in the early works that the type of sulfate source significantly influences the initial rate of C_3A hydration and the identity and transformation rate of AFm phases because of the variation in their solubility [54–56]. C_3A hydration is considered as a concomitant process of surface reactions coupled with the dissolution, precipitation and diffusion phenomena, that contribute equally to the overall hydration [57]. A limited number of studies have also focused on the role of cation-specific effects on the dissolution of sulfate source and its influence on C_3A hydration [36,37,58,59]. When one compares the residual amount of C_3A in sample C93_S7_L0 and C67_S33_L0, it is clear that the hydration is more strongly inhibited with higher amounts of sulfates in the paste.

There are also reports of studies that explored the role of carbonates on the rate of C_3A hydration and found out that it can somehow control the setting time [7,12]. Many studies also focused on the role of carbonates in combination with gypsum in suitable proportions to regulate the C_3A hydration rate [13,17,60,61]. An anion-specific effect on the inhibition of C_3A hydration has been detected in our study and hypothesised to be related to a faster anhydrite dissolution kinetics compared to a slower limestone dissolution. A recent study has revealed that C_3A has an extremely fast dissolution rate within the instantaneous contact with water and are several orders of magnitude greater than that of gypsum or calcite [57]. Both the anhydride dissolution and C_3A hydration starts instantaneously when they are in contact with water. However, as time passes the dissolution rate of C_3A decreases in the presence of anhydrite in a binary formulation. On the other hand, when limestone is present in a binary formulation, C_3A hydration is promoted compared to the anhydrite based binary formulation. This trend is clearly confirmed when one compares phase assemblage of sample C93_S7_L0 and C73_S0_L27 at 28 days (Table 2).

When limestone is added to a C_3A and anhydrite mixture, two competing hydration reactions may take place, calcium carbonate with C_3A and calcium sulfate with C_3A. The hydration behaviour of ternary system involving C_3A, anhydrite and limestone are entirely different from what is reported for other ternary systems involving different forms of calcium sulfate and calcium carbonate. The rate controlling step would be the dissociation into their respective ions as well as their individual amounts. Gismera-Diez et al. reported that when the gypsum and calcite content was low, monosulfate and hemicarbonate was precipitated during C_3A hydration [13].

In the present study, however, metastable phases such as monosulfate and hemicarbonate along with stable phase C_3AH_6 have been jointly precipitated with ettringite and monocarbonate from day 1 in the ternary mixture (sample C72_S13_L15). As the hydration progressed, more sulfate and carbonate ions have been available in the blend which are expected to destabilise both monosulfate and hemicarbonate. Nevertheless, the very same phases that appeared at the commencement of hydration have been detected even after 28 days albeit in different

amounts. When C_3A is hydrated in a binary formulation either with anhydrite or with limestone, hydrogarnet is formed. Similar trend is also witnessed in ternary formulation involving both anhydrite and limestone confirming the acceleration of hydrogarnet formation. Therefore, it can be stated that both anhydrite and limestone partially acted as a filler that would provide nucleation sites for the crystallization of C_3AH_6. The presence of limestone did not completely destabilize either AFm phases or hydrogarnet in sample C72_S13_L15 which are not expected when residual calcium sulfate or calcium carbonate are present in the phase assemblage [62,63]. This behaviour is a consequence of the fact that these phases experience a wider range of thermodynamic stabilities in a combined anhydrite and limestone based formulations (Table S3).

5. Conclusions

The molecular mechanism of the AFm phase formation during C_3A hydration, in the combined presence of anhydrite as well as limestone, and the consequent evolution and stability mapping of calcium aluminate hydrates are successfully established in this study. Hydration products such as C_3AH_6, ettringite and crystalline/amorphous monoanionic AFm phases such as monosulfate, monocarbonate and hydroxy-AFm as well as bi-anionic AFm phases and solid solutions involving hydroxyls, sulfates and carbonates have been detected and quantified. A thorough understanding of the development of these phases, their transitional stability as well as their long-term co-existence are accounted. Furthermore, an anion-specific effect on the inhibition of C_3A hydration was detected.

Although the carbonate ions moderately impede the C_3A dissolution and the precipitation of hydration products in binary formulations, its influence is significantly lower than what is accounted for the sulfate ions. Moreover, limestone can promote the hydration of C_3A in presence of $CaSO_4$ through the formation of ettringite as well as AFm phases and control the setting process and accelerate strength development. The significant increase in the overall C_3A hydration degree in ternary system is hypothesised to be due to the presence of anhydrite and limestone that are partially acting as a filler which would provide nucleation sites for the crystallization of C_3AH_6. However, the dissolved anhydrite and limestone would actively participate in the C_3A hydration process leading to the precipitation of ettringite, monosulfate, monocarbonate and hemicarbonate as well as solid-solutions.

Another important aspect of the present study is to highlight the fact that the hydration of a complicated ternary system can be successfully followed by a combination of complimentary characterization techniques such as MAS NMR spectroscopy and PXRD. We propose the beneficial combined characterization approaches for investigating AFm based solid-solutions involving sulfate, carbonate and hydroxide anions that are precipitated as microcrystalline/amorphous phases. This account delivers further insights into the understanding of the mineralogically and chemically complex phase assemblages generated by the hydration of C_3A in the presence of sulfates and carbonates.

CRediT authorship contribution statement

Valentino Merlo: Methodology, Investigation. **Leonardo Marchese:** Supervision, Writing – review & editing. **Daniela Gastaldi:** Conceptualization, Methodology, Supervision, Writing – review & editing, Visualization. **Enrico Boccaleri:** Supervision, Writing – review & editing, Project administration. **Fulvio Canonico:** Supervision, Project administration. **Geo Paul:** Conceptualization, Methodology, Investigation, Writing – original draft, Visualization.

Declaration of Competing Interest

The authors declare that they have no known competing financial interests or personal relationships that could have appeared to influence the work reported in this paper.

Data availability

No data was used for the research described in the article.

Acknowledgments

This research did not receive any specific grant from funding agencies in the public, commercial, or not-for-profit sectors.

Appendix A. Supplementary data

Supplementary data to this article can be found online at https://doi.org/10.1016/j.conbuildmat.2023.131028.

References

[1] E. Breval, C_3A hydration, Cem. Concr. Res. 6 (1976) 129–137, https://doi.org/10.1016/0008-8846(76)90057-0.
[2] J.W. Bullard, H.M. Jennings, R.A. Livingston, A. Nonat, G.W. Scherer, J. S. Schweitzer, K.L. Scrivener, J.J. Thomas, Mechanisms of cement hydration, Cem. Concr. Res. 41 (2011) 1208–1223, https://doi.org/10.1016/j.cemconres.2010.09.011.
[3] P.W. Brown, L.O. Liberman, G. Frohnsdorff, Kinetics of the Early Hydration of Tricalcium Aluminate in Solutions Containing Calcium Sulfate, J. Am. Ceram. Soc. 67 (1984) 793–795, https://doi.org/10.1111/j.1151-2916.1984.tb19702.x.
[4] J. Skalny, M.E. Tadros, Retardation of Tricalcium Aluminate Hydration by Sulfates, J. Am. Ceram. Soc. 60 (1977) 174–175, https://doi.org/10.1111/j.1151-2916.1977.tb15503.x.
[5] J. Skibsted, H. Bildsøe, H.J. Jakobsen, High-speed spinning versus high magnetic field in MAS NMR of quadrupolar nuclei. ^{27}Al MAS NMR of $3CaO{\cdot}Al_2O_3$, J. Magn. Reson. 1969 (92) (1991) 669–676, https://doi.org/10.1016/0022-2364(91)90367-3.
[6] J. Pommersheim, J. Chang, Kinetics of hydration of tricalcium aluminate, Cem. Concr. Res. 16 (1986) 440–450, https://doi.org/10.1016/0008-8846(86)90120-1.
[7] B. El Elaouni, M. Benkaddour, Hydration of C_3A in the presence of $CaCO_3$, J. Therm. Anal. 48 (1997) 893–901, https://doi.org/10.1007/BF01997194.
[8] J. Skibsted, E. Henderson, H.J. Jakobsen, Characterization of calcium aluminate phases in cements by aluminum-27 MAS NMR spectroscopy, Inorg. Chem. 32 (1993) 1013–1027, https://doi.org/10.1021/ic00058a043.
[9] X. Wang, Y. Pang, H. Lou, Y. Deng, X. Qiu, Effect of calcium lignosulfonate on the hydration of the tricalcium aluminate–anhydrite system, Cem. Concr. Res. 42 (2012) 1549–1554, https://doi.org/10.1016/j.cemconres.2012.08.008.
[10] A. Ramírez, J. Pauli, B. Mota, C. Casselt, S. Simon, W. Schmidt, U. Resch-Genger, C_3A passivation with gypsum and hemihydrate monitored by optical spectroscopy, Cem. Concr. Res. 133 (2020), 106082, https://doi.org/10.1016/j.cemconres.2020.106082.
[11] A.P. Kirchheim, V. Fernàndez-Altable, P.J.M. Monteiro, D.C.C. Dal Molin, I. Casanova, Analysis of cubic and orthorhombic C_3A hydration in presence of gypsum and lime, J. Mater. Sci. 44 (2009) 2038–2045, https://doi.org/10.1007/s10853-009-3292-3.
[12] J. Bensted, Some hydration investigations involving portland cement-effect of calcium carbonate substitution of gypsum, World Cem. Technol. 11 (1980) 395–406.
[13] S. Gismera-Diez, B. Manchobas-Pantoja, P.M. Carmona-Quiroga, M.T. Blanco-Varela, Effect of $BaCO_3$ on C_3A hydration, Cem. Concr. Res. 73 (2015) 70–78, https://doi.org/10.1016/j.cemconres.2015.03.009.
[14] I. Janotka, S.C. Mojumdar, Degree of hydration in cement paste and C_3A-sodium carbonate-water systems, J. Therm. Anal. Calorim. 90 (2007) 645–652, https://doi.org/10.1007/s10973-007-8517-6.
[15] A. Ipavec, R. Gabrovšek, T. Vuk, V. Kaučič, J. Maček, A. Meden, Carboaluminate Phases Formation During the Hydration of Calcite-Containing Portland Cement, J. Am. Ceram. Soc. 94 (2011) 1238–1242, https://doi.org/10.1111/j.1551-2916.2010.04201.x.
[16] G. Kakali, S. Tsivilis, E. Aggeli, M. Bati, Hydration products of C_3A, C_3S and Portland cement in the presence of $CaCO_3$, Cem. Concr. Res. 30 (2000) 1073–1077, https://doi.org/10.1016/S0008-8846(00)00292-1.
[17] Y. Zhang, X. Zhang, Research on effect of limestone and gypsum on C_3A, C_3S and PC clinker system, Constr. Build. Mater. 22 (2008) 1634–1642, https://doi.org/10.1016/j.conbuildmat.2007.06.013.
[18] Cement industry events, news & research - Global Cement, (n.d.). https://www.globalcement.com/ (accessed June 8, 2021).
[19] European Committee for Standardization, Cement — Part 1: Composition, Specifications and Conformity Criteria for Common Cements, EN 197-1, 2000, n.d.
[20] G. Paul, E. Boccaleri, L. Buzzi, F. Canonico, D. Gastaldi, Friedel's salt formation in sulfoaluminate cements: A combined XRD and ^{27}Al MAS NMR study, Cem. Concr. Res. 67 (2015) 93–102, https://doi.org/10.1016/j.cemconres.2014.08.004.
[21] D. Gastaldi, G. Paul, L. Marchese, S. Irico, E. Boccaleri, S. Mutke, L. Buzzi, F. Canonico, Hydration products in sulfoaluminate cements: Evaluation of

amorphous phases by XRD/solid-state NMR, Cem. Concr. Res. 90 (2016) 162–173, https://doi.org/10.1016/j.cemconres.2016.05.014.
[22] D. Gastaldi, F. Bertola, F. Canonico, L. Buzzi, S. Mutke, S. Irico, G. Paul, L. Marchese, E. Boccaleri, A chemical/mineralogical investigation of the behavior of sulfoaluminate binders submitted to accelerated carbonation, Cem. Concr. Res. 109 (2018) 30–41, https://doi.org/10.1016/j.cemconres.2018.04.006.
[23] S. Irico, A.G. Bovio, G. Paul, E. Boccaleri, D. Gastaldi, L. Marchese, L. Buzzi, F. Canonico, A solid-state NMR and X-ray powder diffraction investigation of the binding mechanism for self-healing cementitious materials design: The assessment of the reactivity of sodium silicate based systems, Cem. Concr. Compos. 76 (2017) 57–63, https://doi.org/10.1016/j.cemconcomp.2016.11.006.
[24] G. Paul, E. Boccaleri, L. Marchese, L. Buzzi, F. Canonico, D. Gastaldi, Low temperature sulfoaluminate clinkers: The role of sulfates and silicates on the different hydration behavior, Constr. Build. Mater. 268 (2021), 121111, https://doi.org/10.1016/j.conbuildmat.2020.121111.
[25] D. Gastaldi, F. Bertola, S. Irico, G. Paul, F. Canonico, Hydration behavior of cements with reduced clinker factor in mixture with sulfoaluminate binder, Cem. Concr. Res. 139 (2021), 106261, https://doi.org/10.1016/j.cemconres.2020.106261.
[26] B. Walkley, J.L. Provis, Solid-state nuclear magnetic resonance spectroscopy of cements, Mater. Today Adv. 1 (2019), 100007, https://doi.org/10.1016/j.mtadv.2019.100007.
[27] A. Wesselsky, O.M. Jensen, Synthesis of pure Portland cement phases, Cem. Concr. Res. 39 (2009) 973–980, https://doi.org/10.1016/j.cemconres.2009.07.013.
[28] G. Paul, C. Bisio, I. Braschi, M. Cossi, G. Gatti, E. Gianotti, L. Marchese, Combined solid-state NMR, FT-IR and computational studies on layered and porous materials, Chem. Soc. Rev. 47 (2018) 5684–5739, https://doi.org/10.1039/C7CS00358G.
[29] D. Massiot, F. Fayon, M. Capron, I. King, S.L. Calvé, B. Alonso, J.-O. Durand, B. Bujoli, Z. Gan, G. Hoatson, Modelling one- and two-dimensional solid-state NMR spectra, Magn. Reson. Chem. 40 (2002) 70–76, https://doi.org/10.1002/mrc.984.
[30] J. Skibsted, H.J. Jakobsen, Characterization of the Calcium Silicate and Aluminate Phases in Anhydrous and Hydrated Portland Cements by ^{27}Al and ^{29}Si MAS NMR Spectroscopy, in: P. Colombet, H. Zanni, A.-.-R. Grimmer, P. Sozzani (Eds.), Nucl. Magn. Reson. Spectrosc, Cem.-Based Mater., Springer, Berlin, Heidelberg, 1998, pp. 3–45, https://doi.org/10.1007/978-3-642-80432-8_1.
[31] J.-B. d'Espinose de Lacaillerie, C. Fretigny, D. Massiot, MAS NMR spectra of quadrupolar nuclei in disordered solids: The Czjzek model, J. Magn. Reson. 192 (2008) 244–251, https://doi.org/10.1016/j.jmr.2008.03.001.
[32] F. Bertola, D. Gastaldi, S. Irico, G. Paul, F. Canonico, Behavior of blends of CSA and Portland cements in high chloride environment, Constr. Build. Mater. 262 (2020), 120852, https://doi.org/10.1016/j.conbuildmat.2020.120852.
[33] M.J. Sánchez-Herrero, A. Fernández-Jiménez, A. Palomo, D. Viehland, Alkaline Hydration of Tricalcium Aluminate, J. Am. Ceram. Soc. 95 (10) (2012) 3317–3324.
[34] M.A.G. Aranda, A. Cuesta, A.G.D. la Torre, I. Santacruz, L. León-Reina, 2. Diffraction and crystallography applied to hydrating cements, De Gruyter, 2017. https://www.degruyter.com/document/doi/10.1515/9783110473728-003/html (accessed June 8, 2021).
[35] X. Liu, P. Feng, C. Lyu, S. Ye, The role of sulfate ions in tricalcium aluminate hydration: New insights, Cem. Concr. Res. 130 (2020), 105973, https://doi.org/10.1016/j.cemconres.2020.105973.
[36] A.S. Brand, S.B. Feldman, P.E. Stutzman, A.V. Ievlev, M. Lorenz, D.C. Pagan, S. Nair, J.M. Gorham, J.W. Bullard, Dissolution and initial hydration behavior of tricalcium aluminate in low activity sulfate solutions, Cem. Concr. Res. 130 (2020), 105989, https://doi.org/10.1016/j.cemconres.2020.105989.
[37] A. Quennoz, K.L. Scrivener, Hydration of C_3A–gypsum systems, Cem. Concr. Res. 42 (2012) 1032–1041, https://doi.org/10.1016/j.cemconres.2012.04.005.
[38] G. Paul, E. Boccaleri, C. Cassino, D. Gastaldi, L. Buzzi, F. Canonico, L. Marchese, Fingerprinting the Hydration Products of Hydraulic Binders Using Snapshots from Time-Resolved In Situ Multinuclear MAS NMR Spectroscopy, J. Phys. Chem. C. 125 (2021) 9261–9272, https://doi.org/10.1021/acs.jpcc.1c00984.
[39] J. Skibsted, M.T. Pedersen, J. Holzinger, Resolution of the Two Aluminum Sites in Ettringite by ^{27}Al MAS and MQMAS NMR at Very High Magnetic Field (22.3 T), J. Phys. Chem. C. 121 (2017) 4011–4017, https://doi.org/10.1021/acs.jpcc.6b11875.
[40] M.M. Radwan, M. Heikal, Hydration characteristics of tricalcium aluminate phase in mixes containing β-hemihydate and phosphogypsum, Cem. Concr. Res. 35 (2005) 1601–1608, https://doi.org/10.1016/j.cemconres.2004.06.037.
[41] P. Faucon, T. Charpentier, D. Bertrandie, A. Nonat, J. Virlet, J.C. Petit, Characterization of Calcium Aluminate Hydrates and Related Hydrates of Cement Pastes by ^{27}Al MQ-MAS NMR, Inorg. Chem. 37 (1998) 3726–3733, https://doi.org/10.1021/ic9800076.
[42] A. Mesbah, C. Cau-dit-Coumes, F. Frizon, F. Leroux, J. Ravaux, G. Renaudin, A New Investigation of the Cl^-–CO_3^{2-} Substitution in AFm Phases, J. Am. Ceram. Soc. 94 (2011) 1901–1910, https://doi.org/10.1111/j.1551-2916.2010.04305.x.
[43] J. Xiao, C. Gou, Y. Jin, Y. Wang, Effect of $CaCO_3$ on hydration characteristics of C_3A, J. Cent. South Univ. Technol. 17 (2010) 918–923, https://doi.org/10.1007/s11771-010-0577-2.
[44] T. Matschei, B. Lothenbach, F.P. Glasser, The AFm phase in Portland cement, Cem. Concr. Res. 37 (2007) 118–130, https://doi.org/10.1016/j.cemconres.2006.10.010.
[45] H.-J. Kuzel, H. Pöllmann, Hydration of C_3A in the presence of $Ca(OH)_2$, $CaSO_4{\cdot}2H_2O$ and $CaCO_3$, Cem. Concr. Res. 21 (1991) 885–895, https://doi.org/10.1016/0008-8846(91)90183-I.
[46] B. Lothenbach, G. Le Saout, E. Gallucci, K. Scrivener, Influence of limestone on the hydration of Portland cements, Cem. Concr. Res. 38 (2008) 848–860, https://doi.org/10.1016/j.cemconres.2008.01.002.
[47] M.A. Trezza, A.E. Lavat, Analysis of the system $3CaO{\cdot}Al_2O_3$–$CaSO_4{\cdot}2H_2O$–$CaCO_3$–H_2O by FT-IR spectroscopy, Cem. Concr. Res. 31 (2001) 869–872, https://doi.org/10.1016/S0008-8846(01)00502-6.
[48] T. Runčevski, R.E. Dinnebier, O.V. Magdysyuk, H. Pöllmann, Crystal structures of calcium hemicarboaluminate and carbonated calcium hemicarboaluminate from synchrotron powder diffraction data, Acta Crystallogr. B. 68 (2012) 493–500, https://doi.org/10.1107/S010876811203042X.
[49] G. Renaudin, M. Francois, O. Evrard, Order and disorder in the lamellar hydrated tetracalcium monocarboaluminate compound, Cem. Concr. Res. 29 (1999) 63–69, https://doi.org/10.1016/S0008-8846(98)00184-7.
[50] M. François, G. Renaudin, O. Evrard, A Cementitious Compound with Composition $3CaO.Al_2O_3.CaCO_3.11H_2O$, Acta Crystallogr. C. 54 (1998) 1214–1217, https://doi.org/10.1107/S0108270198004223.
[51] D. Damidot, S. Stronach, A. Kindness, M. Atkins, F.P. Glasser, Thermodynamic investigation of the CaO-Al_2O_3-$CaCO_3$-H_2O closed system at 25°C and the influence of Na_2O, Cem. Concr. Res. 24 (1994) 563–572, https://doi.org/10.1016/0008-8846(94)90145-7.
[52] L.G. Baquerizo, T. Matschei, K.L. Scrivener, M. Saeidpour, L. Wadsö, Hydration states of AFm cement phases, Cem. Concr. Res. 73 (2015) 143–157, https://doi.org/10.1016/j.cemconres.2015.02.011.
[53] J. Goergens, T. Manninger, F. Goetz-Neunhoeffer, In-situ XRD study of the temperature-dependent early hydration of calcium aluminate cement in a mix with calcite, Cem. Concr. Res. 136 (2020), 106160, https://doi.org/10.1016/j.cemconres.2020.106160.
[54] S. Pourchet, L. Regnaud, J.P. Perez, A. Nonat, Early C_3A hydration in the presence of different kinds of calcium sulfate, Cem. Concr. Res. 39 (2009) 989–996, https://doi.org/10.1016/j.cemconres.2009.07.019.
[55] F.J. Tang, E.M. Gartner, Influence of sulphate source on Portland cement hydration, Adv. Cem. Res. 1 (1988) 67–74, https://doi.org/10.1680/adcr.1988.1.2.67.
[56] J. Bensted, Effects of the clinker - gypsum grinding temperature upon early hydration of Portland cement, Cem. Concr. Res. 12 (1982) 341–348, https://doi.org/10.1016/0008-8846(82)90082-5.
[57] S. Ye, P. Feng, Y. Liu, J. Liu, J.W. Bullard, In situ nano-scale observation of C_3A dissolution in water, Cem. Concr. Res. 132 (2020), 106044, https://doi.org/10.1016/j.cemconres.2020.106044.
[58] M. Collepardi, G. Baldini, M. Pauri, M. Corradi, Tricalcium aluminate hydration in the presence of lime, gypsum or sodium sulfate, Cem. Concr. Res. 8 (1978) 571–580, https://doi.org/10.1016/0008-8846(78)90040-6.
[59] B.A. Clark, P.W. Brown, The formation of ettringite from tricalcium aluminate and magnesium sulphate, Adv. Cem. Res. 12 (2000) 137–142, https://doi.org/10.1680/adcr.2000.12.4.137.
[60] C.A. Utton, E. Gallucci, J. Hill, N.B. Milestone, Interaction between $BaCO_3$ and OPC/BFS composite cements at 20 °C and 60 °C, Cem. Concr. Res. 41 (2011) 236–243, https://doi.org/10.1016/j.cemconres.2010.11.006.
[61] W. Han, T. Sun, X. Li, Z. Shui, Y. Chen, M. Sun, Influence of Lithium Carbonate on C_3A Hydration, Adv. Mater. Sci. Eng. 2018 (2018) e6120269.
[62] T. Matschei, F.P. Glasser, Temperature dependence, 0 to 40 °C, of the mineralogy of Portland cement paste in the presence of calcium carbonate, Cem. Concr. Res. 40 (2010) 763–777, https://doi.org/10.1016/j.cemconres.2009.11.010.
[63] M.U. Okoronkwo, F.P. Glasser, Compatibility of hydrogarnet, $Ca_3Al_2(SiO_4)_x(OH)_{4(3-x)}$, with sulfate and carbonate-bearing cement phases: 5–85 °C, Cem. Concr. Res. 83 (2016) 86–96, https://doi.org/10.1016/j.cemconres.2016.01.013.